Journal of Magnetic Resonance 210 (2011) 44–50

Contents lists available at ScienceDirect

Journal of Magnetic Resonance

journal homepage: www.elsevier.com/locate/jmr

Rectangular loop-gap resonator with the light access to the sample

Małgorzata Dutka [a,*], Tadeusz Oleś [a], Marek Mossakowski [a,b], Wojciech Froncisz [a]

[a] Department of Biophysics, Faculty of Biochemistry, Biophysics and Biotechnology, Jagiellonian University, Gronostajowa 7, 30-387 Kraków, Poland
[b] Department of Electronics, AGH University of Science and Technology, Al. Mickiewicza 30, 30-059 Kraków, Poland

ARTICLE INFO

Article history:
Received 29 December 2010
Available online 1 March 2011

Keywords:
Continuous wave electron paramagnetic resonance
Rectangular loop gap resonator
Resonator with light access
Microwave magnetic field distribution

ABSTRACT

A modified rectangular loop-gap resonator for X-band electron paramagnetic resonance (EPR) studies of aqueous samples, enabling the light access, is described. Changes introduced into rectangular resonator geometry, previously presented in Piasecki et al. (1998) [1], and redesigned coupling structure lead to the better thermal and mechanical stability. The modified structure makes provision for the controlled light access to the sample placed in a flat cell during an EPR experiment. The sensitivity of the resonator for aqueous samples as well as an experimentally tested microwave magnetic field homogeneity are presented. Results of simulations and experimental tests indicate that the presence of light access holes in the resonator's front side does not disturb the uniformity of microwave magnetic field distribution in the nodal plane. The optimal flat cell thickness for unsaturable and saturable aqueous samples has been calculated for this new structure. A modified rectangular geometry of the loop-gap resonator ensures a good performance for aqueous samples allowing its convenient and efficient light illumination during EPR signal recording .

1. Introduction

Among the entire range of proposed loop-gap resonators [2] the 1 mm cylindrical two-loop-one gap resonator found the widest application in biophysical studies of proteins [3]. Many EPR studies of the structure and dynamics of proteins using the side directed spin labeling (SDSL) were performed with that resonator [4,5]. In spite of many attractive features of that resonator its small active volume (about 1.6 μL) is impractical for some EPR experiments. Moreover, the light illumination of the sample is not an easy task for that loop-gap geometry which complicates EPR studies of conformational changes of proteins induced by the light.

The most commonly used resonators for the EPR spectroscopy of aqueous samples are the rectangular TE_{102} and cylindrical TM_{110} cavities. The presence of a nodal plane for the electric field in the center of those cavities allows the use of a flat cell instead of capillary as a aqueous sample container. It is rather a simple task to provide the light access to the sample for those cavities. Their active sample volume is however rather high and exceeds 50 μL.

In the attempt to find an alternative to the rectangular and cylindrical cavities with the smaller active sample volume we recently proposed a novel loop-gap resonator with a rectangular central loop. In that resonator, the optimum performance was achieved for a six-gap-seven-loop structure [1]. The experimental results were obtained with the resonator made of a single piece of silver plated Macor™. This gave an EPR signal amplitude comparable to the TE_{102} cavity with a much smaller sample volume of only 16 μL. In practical applications of the rectangular loop-gap resonator, aqueous solutions of spin-labeled proteins were placed into the quartz flat cell with a 0.4 mm by 4 mm cross-section [6]. However, the size and complexity of that structure were causing various practical problems. It was difficult to machine the resonator and its mechanical and thermal stability was rather problematic giving rise to the unstable baseline of the EPR spectrum. Moreover, it was impossible to provide the light to the sample in that structure.

In the present paper we describe an improved version of the rectangular loop-gap resonator with similar active sample volume which gives slightly higher sensitivity for aqueous samples. A modification of a basic construction has been introduced to provide the convenient light access to the sample, contained in a transparent flat cell with dimensions matched to the inner space of the resonator. Owing to that the light-induced transient phenomena can be monitored directly via simultaneously recorded EPR signal changes. The light exposed surface of the sample cell in the active volume exceeds 50%. Thus the ratio of the photoexcitable volume to the entire volume of the sample is very advantageous.

2. Instrumentation

An exploded and cross-sectional views of the resonator are presented in Figs. 1 and 2 and key resonator dimensions are given in

* Corresponding author. Fax: +48 12 664 69 02.
E-mail addresses: Malgorzata.Dutka@uj.edu.pl (M. Dutka), Tadeusz.Oles@uj.edu.pl (T. Oleś), Marek.Mossakowski@agh.edu.pl (M. Mossakowski), Wojciech.Froncisz@uj.edu.pl (W. Froncisz).

1090-7807/$ - see front matter © 2011 Elsevier Inc. All rights reserved.
doi:10.1016/j.jmr.2011.02.009

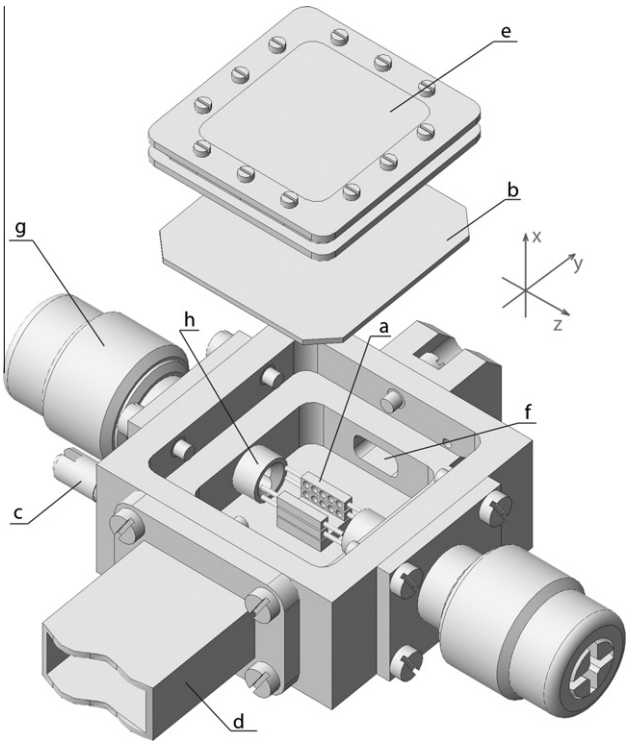

Fig. 1. The structure of the modified RLGR resonator: (a) rectangular brass rods with holes for light access; (b) side wall; (c) coupling screw; (d) rectangular waveguide; e-modulation coil; (f) opening for the light access light window; (g) sample access stack; (h) Rexolite holder.

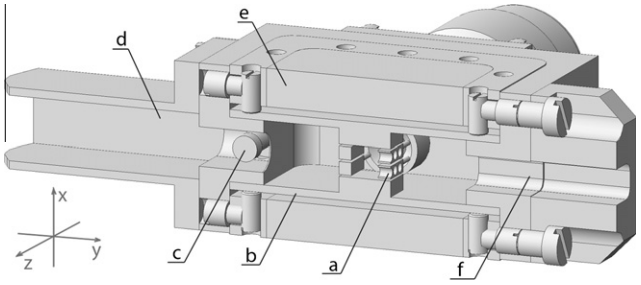

Fig. 2. Cross-section view of the resonator. The same elements like in Fig. 1 are pointed.

Table 1. It is a three-loop-six-gap structure. The main body of the resonator is made of silver plated brass. The capacitive part of the resonator is formed by four rectangular silver plated brass rods suspended in space by the phosphor bronze wires that are supported by two Rexolite™ holders on the top and bottom of the resonator body (Fig. 1). In order to provide the magnetic field modulation to the sample the opening sides of the resonator body are covered with the side walls made of silver plated unclad laminate used for PCB. The magnetic field modulation is provided by the modulation coils attached to the resonator body (Fig. 2).

In order to provide an access of light to the sample the rectangular opening was made in the front part of the brass body and additional five holes with 1.5 mm I.D. were made in each of two front rectangular rods that form the resonator's capacitance (Fig. 1). Those ten holes together with the vertical slot, that plays the role of the central resonator gap, cause that the light exposed surface exceeds 50% of the sample active area. That arrangement allows illumination of the flat sample cell placed in the center of the resonator as is shown in the front view of the resonator.

Table 1
Technical parameters of the rectangular loop-gap resonator with redesigned coupling structure and direct light access to the sample.

Gap width	2.0 mm
Gap separation	0.35 mm
Gap height	10.0 mm
Central loop width	5.1 mm
Central loop length	4.5 mm
Return flux loop width	10.0 mm
Return flux loop length	12.3 mm
Internal height of the body	30.0 mm
External height of the body without the sample access stack	54.0 mm
External height of the body with the sample access stack above and below the resonator	102.0 mm
External width of the body	26.0 mm
External length of the body	54.0 mm
Resonant frequency (ν_0)	9.55 GHz
Unloaded (Q)	3100
Microwave efficiency (Λ)	2.5 G/W$^{1/2}$

The resonator is coupled directly to the waveguide through the coupling structure that resembles the Varian coupler, with a metal slug moving down over the slot cut parallel to the axis of the rectangular loop as described previously [7] .

The sample access stacks above and below the resonator have Bruker standard dimensions thus the Bruker collet system can be used.

The electrical properties were tested on the bench using a microwave setup equipped with the microwave sweeper. The EPR measurements were performed using either the home made pulse EPR spectrometer [8] or Bruker ESP 300E spectrometer.

The cuvettes used for aqueous samples were either flat glass capillaries (width 4 mm, thickness 0.4 mm, Vitro Dynamics, Inc., Rockaway, NJ) or flat cells with the same internal dimensions made of plexiglass or TPX at the laboratory.

The microwave efficiency, Λ, was measured using the technique of perturbing metal spheres [9], in combination with EPR measurements of the small speck of DPPH (2α-diphenyl-β-picrylhydrazil).

The light-induced experiments were performed on the sample containing synthetic dopa-melanin dissolved in 0.1M phosphate buffer, pH 8.0, at the concentration of 2 mg/mL [10]. Illumination of that sample with the visible light considerably increases the amplitude of the melanin EPR spectrum [11].

3. Performance and analysis

Technical data of the resonator are presented in Table 1. As can be seen from Table 1 the dimensions of the central rectangular loop are slightly bigger then in the previous version of the rectangular loop-gap resonator [1]. The reason for doing this was to broaden applicability of the resonator for a standard 4 mm O.D. tube, e.g. a pitch sample.

The most dramatic improvement of the resonator is observed for its quality factor, Q. The loaded quality factor of the empty Macor™ resonator was 550 [1], while for the present resonator its Q exceeds 1500 (Table 1). That threefold increase of the Q value led to the much higher microwave efficiency parameter Λ that reaches 2.5 G/$\sqrt{W}$.

The question arises why the Q value for the new resonator is so much higher than in the previous one? Three factors can be pointed out that contribute to so substantial increase of the Q value.

It seems that the main factor can be related to a different geometry of the return flux loops. There were six loops that house the return flux in the previous Macor resonator [1], while there are

only two ones in the modified rectangular loop-gap resonator. Assuming the same B_1 in the return flux loops for both resonators, the microwave current density is also the same. However, the length of the current path is three times bigger in the Macor resonator in comparison with the new one causing that an equivalent resistance is also three times higher. It follows that the losses produced by the current flowing on the surface of the return flux loops are threefold higher.

The second reason can be related to the poorer quality of the conductive surface formed by the silver deposition on the Macor in comparison with the silver plated brass that can be machined more precisely.

Finally, some contribution to higher losses in the previous resonator can be attributed to the different coupling structure. The previous resonator was coupled to the coaxial transmission line using the coupling loop, while the new resonator is coupled directly to the waveguide with the use of a hole between waveguide and one of the return flux loops.

Boring holes in front panels of the resonator may change properties and characteristics of the resonator. The microwave magnetic field uniformity was tested experimentally in the nodal plane of the resonator using a speck of DPPH. The position of the sample in the nodal plane was controlled with the use of a specially constructed tube holder that allows testing the distribution of the EPR signal amplitude for a point sample along three lines parallel to the resonator vertical axis *Oz*. While the microwave power incident upon the cavity is kept constant, we are observing dependence of the signal intensity on the point sample position. Obviously, the EPR signal at resonance – equivalent to the amount of microwave power absorbed by spins – is proportional to $\langle B_1^2 \rangle$, square of the microwave magnetic field averaged over the sample volume.

The experimental signal amplitude was corrected in order eliminate the magnetic modulation field inhomogeneity within the cavity (determined independently).

The results are presented in Fig. 3 for two resonators, one without the light access holes in the brass rods, and another with five 1.5 mm I.D. holes in each of two rods. To our surprise, the microwave magnetic field distribution in the nodal plane of the resonator seems to be unchanged by the presence of holes that are altering conductive surfaces that support the flow of microwave currents. In both resonators the microwave magnetic field distribution is very uniform in the nodal plane making them excellent for the EPR experiments.

Results of measurements are supported by simulation of three dimensional distribution of the electromagnetic field for the resonator with holes. The high frequency structure simulator Ansoft(R) HFSS 11.0 installed on PC with i7, 3 GHz, 8 GB RAM,

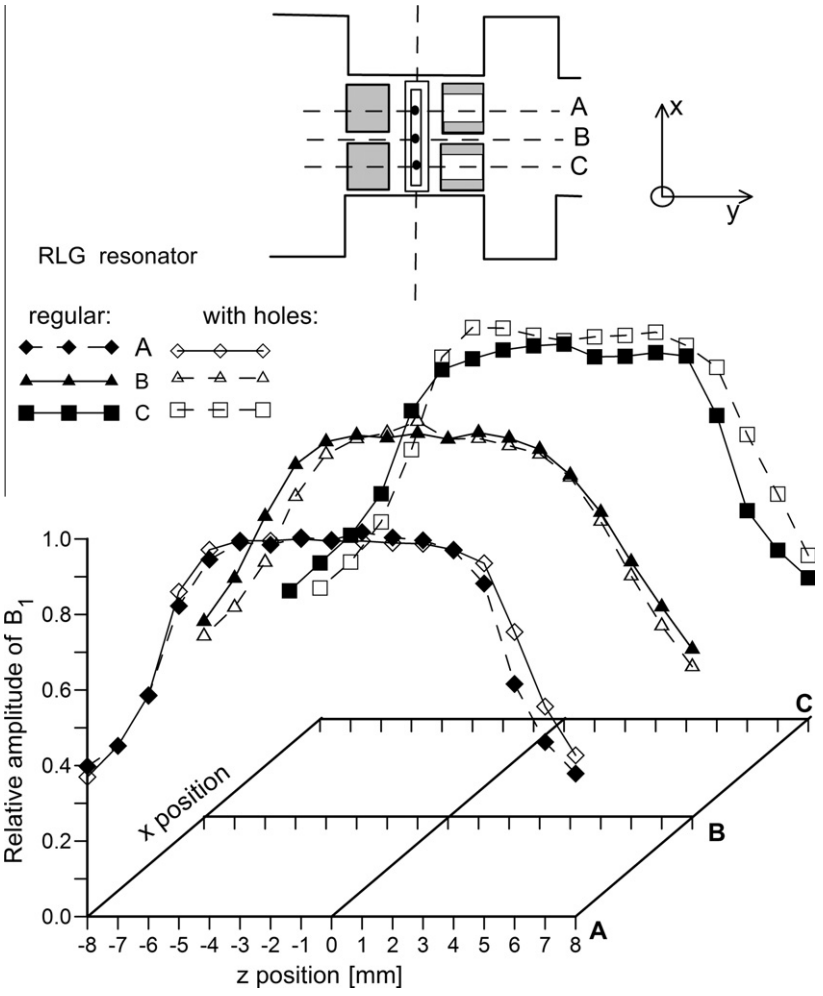

Fig. 3. The microwave magnetic field distribution measured along the nodal plane of the rectangular resonator with the point DPPH sample. B_1 amplitude is normalized with respect to the value at the geometrical center (0, 0, 0). Data have been collected for basic rectangular loop-gap resonator and modified one: with holes enabling the light access. The upper inset presents the schematic transversal cross-section of the resonator body with the tube holder within, used for controlling the point sample position during the measurements.

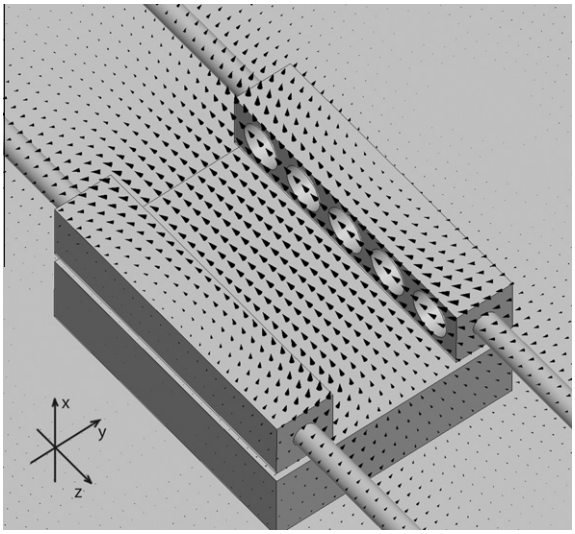

Fig. 4. Distribution of the microwave magnetic field inside the modified rectangular loop-gap resonator, obtained from finite-element simulations (Ansoft® HFSS™ 11.0). Magnetic field vectors in a plane bisecting the resonator along *Oy* direction are shown.

was used. The visualization of the magnitude and direction of the microwave magnetic field B_1 is presented in Fig. 4. The field distribution is very uniform in the central rectangular loop in the box of approximate dimensions $2 \times 4 \times 10$ mm and is slightly distorted only in very close proximity of the light holes. Further diagrams show the contour plots of *z*- component of microwave magnetic field (denoted as B_{1Z}), at chosen planar cross-sections of 3D distribution. Applied normalization (with respect to the value of B_1 at the geometrical center of the resonator) allows us to evaluate directly the field uniformity. Fig. 5a reflects simulated B_{1Z} distribution at the nodal plane of the resonator, where the flat sample cuvette is positioned. It is interesting to compare B_{1Z} distributions at planes perpendicular to nodal one. Plots (b) and (c) in Fig. 5 show B_{1Z} distribution at the planes *Oy*–*Oz* passing through the center of the rode (*x*- coordinate equal to 1.2 mm) and in the middle between the rods (*x*- coordinate equal to 0.0 mm) respectively. It is explicitly shown that the range of perturbation in the microwave field uniformity does not expand to the position of the cuvette.

4. Active length of the resonators

Most resonators used in the EPR spectroscopy, with exception of the recently described uniform field resonators [12,13], have more or less non-uniform field distribution along the sample axis. The maximum value of the magnetic component of the microwave field, B_1, occurs in the resonator center and the field decays down to zero at the edge of the resonator. The total EPR signal intensity is proportional to the integral of B_1^2 over the sample volume. Because of the non-uniform $\mathbf{B_1}$ distribution, the contribution of the spins located at the edges of the resonator to the EPR signal intensity is negligible. It is then reasonable to make the sample shorter than the internal height of the resonator especially in the case when the amount of sample is limited as it often happens in the SDSL EPR studies of proteins. The question arises how to choose the optimum sample length for such studies that would define the active length and the active volume of the sample.

We propose here a new definition of an effective sample length as the length of the sample, positioned at the center of the resonator, that gives 90% of the signal intensity that would be if the sample did extended the full height of the resonator.

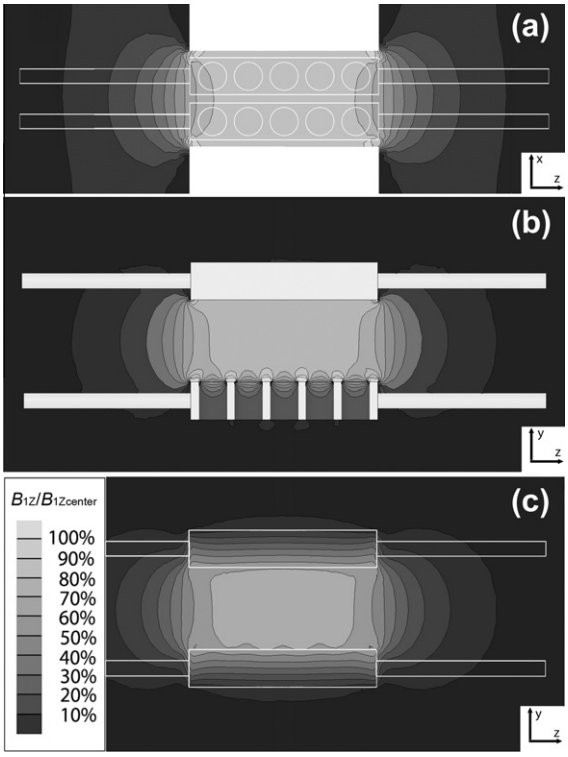

Fig. 5. Contour plots representing simulated values of B_{1Z} component at the different planes crosscutting the resonator. (a) The B_{1Z} distribution along the nodal plane (*Ox*–*Oz*) of the resonator. The schematic layout of the resonator structure (white lines) is superimposed. (b) Visualization of simulated B_{1Z} distribution at *Oy*–*Oz* plane, perpendicular to nodal plane and passing through the middle of the holes in the rod (along to the A′A or C′C directions from Fig. 3). (c). A contour map of simulated B_{1Z} distribution at the central *Oy*–*Oz* plane of the resonator, passing through the vertical slot (equivalent to the B′B direction from Fig. 3).

Defined in that way an active sample length ΔL_{eff} can be determined by integration of B_1^2 over *z*- coordinate, until the ratio of the integrals approaches 0.9:

$$\frac{\int_{-\Delta L_{eff}/2}^{\Delta L_{eff}/2} B_1^2(z) \cdot dz}{\int_{-d}^{d} B_1^2(z) \cdot dz} = 0.9 \tag{1}$$

The internal height of the resonator equals 2*d*.

The $\mathbf{B_1}$ dependence on *z*-coordinate is well described by analytical expressions in case of cavities, i.e. TE_{102}, TM_{110}. It can be also calculated using the high frequency structure simulator for any resonant structure, as was done for the rectangular loop-gap resonator or can be measured experimentally using a speck of DPPH.

In turn, determination of the effective length allows to express the field's non-uniformity by calculating the average B_1^2 over the effective length according to the formula:

$$\overline{B_1^2} = \frac{\int_{-\Delta L_{eff}/2}^{\Delta L_{eff}/2} B_1^2(z) \cdot dz}{\Delta L_{eff}} \tag{2}$$

The ratio of $\overline{B_1^2}$ to $B_{1\,\max}^2$ can be used to describe the degree of the field non-uniformity, δ, for the particular resonator:

$$\delta = \frac{\overline{B_1^2}}{B_{1\,\max}^2} \tag{3}$$

For the perfectly uniform field δ equals 1 and decreases for resonators with the less uniform field distribution.

Table 2
Effective length, ΔL_{eff}, and field uniformity δ calculated for different resonators.

Type of resonator	Internal height of the resonator (mm)	Effective length ΔL_{eff} (mm) which gives 90% of the signal	$\frac{B_1 at\ \Delta L_{eff}/2}{B_{1max}}$	$\delta = \frac{\overline{B_1^2}}{B_{1\max}^2}$
RLGR[a]	30.0	11.7	0.59	0.82
TE_{102}	23.0	13.7	0.60	0.75
TM_{110}[b]	38.5	20.6	0.56	0.72
TE_{U02}[c]	55.5	45.8	1.00	1.00

[a] Rectangular loop-gap resonator described in this paper.
[b] The diameter of the cavity resonating at 9.5 GHz was 38.49 mm.
[c] Rectangular uniform field resonator with L = 46 mm and d = 4.73 mm resonating at 9.5 GHz [11].

Using the above definitions (Eqs. (1) and (3)) the values for active sample length and the magnetic field uniformity were calculated for the rectangular loop-gap resonator of this paper as well as for two most popular cavities: rectangular TE_{102} and cylindrical TM_{110} (Table 2). Additionally the data for the rectangular uniform field resonator are included in the table because that resonator represents the perfect structure in sense of the field uniformity.

5. Non-lossy samples

Hyde [14] introduced a system of sample classification that assigns each EPR sample into one of eight classes on the basis of its saturability, dielectric losses and limitation in size or volume. The rectangular loop-gap resonator presented in this paper was mainly designed for aqueous samples of spin-labeled proteins. Those samples are saturable, exhibit high dielectric losses and usually are limited in size. As it turned out the new resonator is also very useful for samples that do not reveal high dielectrics losses and are not limited in size. This class of samples can be represented by the standard EPR sample – weak pitch. It saturates at moderate microwave powers in cavities and is used by manufacturers to test the sensitivities of the EPR spectrometers. The measurements showed that the new rectangular loop-gap resonator gives 4.3 times higher amplitude for the weak pitch sample than the TM_{110} cavity. This is consistent with the high value of the Λ parameter ($2.5\ G/\sqrt{W}$), effective sample length ΔL_{eff} calculated above and parameter δ of the rectangular loop-gap resonator in comparison with the TM_{110} cavity (Table 2). It follows from the fact that the signal amplitude is proportional to the product of those parameters at the constant observe power. Thus the calculated ratio of the weak pitch amplitude recorded with the rectangular loop-gap resonator (RLGR) to that of cylindrical TM_{110} cavity equals:

$$\frac{\Lambda_{\mathrm{RLGR}}^2 \delta_{\mathrm{RLGR}} \cdot \Delta L_{\mathrm{RLGR}}}{\Lambda_{\mathrm{TM}}^2 \delta_{\mathrm{TM}} \cdot \Delta L_{\mathrm{TM}}} = 4.04 \tag{4}$$

which is very close to the measured value of 4.3. These calculations neglect the field inhomogeneity in the cross-section of the weak pitch sample. This is justified as the results of the high frequency structure simulations show (see Fig. 4 for the RLGR), that the field is very uniform in the cross section of that sample. The value of Λ for TM cavity was taken to be $1G/\sqrt{W}$ according to the Bruker data [15]. Our measurements of the Λ for the Bruker TM_{110} cavity (ER4103TM) using the technique of perturbing metal spheres [9], gave slightly lower value that improves the agreement of calculated ratio with experimental value of 4.3.

Performance comparison of two different resonators for saturable samples requires adjustment of the microwave power until the B_1 value in both resonators is the same. This can be done for the maximum value of B_1 in the center of the resonator or for average value as shown in the Table 2. We consider here the first case and then it is easy to show that the signal amplitude is proportional to the product of Λ, effective length ΔL and δ. Note that for non-saturable samples the signal amplitude is proportional to Λ^2. Thus for saturable line samples, the ratio of the signal amplitude for the RLGR to that for TM_{110} cavity is:

$$\frac{\Lambda_{\mathrm{RLGR}} \delta_{\mathrm{RLGR}} \cdot \Delta L_{\mathrm{RLGR}}}{\Lambda_{\mathrm{TM}} \delta_{\mathrm{TM}} \cdot \Delta L_{\mathrm{TM}}} = 1.6 \tag{5}$$

In terms of sensitivity the RLGR is significantly better than the TM_{110} cavity for both classes of non-lossy, unlimited size samples. For limited size samples those numbers would be almost twice bigger due to nearly two times bigger an effective length of the TM_{110} cavity (Table 2).

6. Lossy samples

As was stated above the main goal of developing of the RLGR was its possible application to studies of saturable aqueous samples which have somewhat limited size. This resonator possesses a nodal plane for the electric component of the microwave field analogous to TE_{102} and TM_{110} cavity. Its microwave field configuration is suitable for the use of the flat cell for aqueous samples. In our previous work the optimum thickness of the flat cell for non-saturable aqueous samples approached 0.4 mm as was determined both theoretically and experimentally [1]. The significantly increased Q value of the modified RLGR, 3100 in comparison with 1100 of the previous RLGR, caused a necessity to find out again the optimum sample thickness for both saturable and non-saturable aqueous samples.

The EPR signal for the reflection resonator employing a linear microwave detector is proportional to the product of the filling factor, η, quality factor, Q, and square root of incident power, P_{in} [16]. Two first parameters, η and Q, describe the physical properties of the resonator itself and are independent on the spectrometer configuration. The incident microwave power depends on the spectrometer and theoretically can be set at any arbitrary level for non-saturable samples. Thus in order to find out the optimum flat cell thickness for non-saturable samples it is customary to keep a constant level of P_{in} and maximize the product of η and Q.

It is worth noting that this procedure is not always justified because of the fact that the noise level of the spectrometer, which originates from the demodulation of the phase noise of the microwave source by the resonator, depends on its Q. Additionally, the level of incident microwave power could be limited by thermal instability of the resonator caused by the excessive dissipation of microwaves in the resonator walls and lossy samples.

The product of η and Q was calculated applying the high frequency structure simulator and taking the complex dielectric constants for water at 25 °C and 9.5 GHz, $\varepsilon_{H_2O} = 55(1 + 0.54 \cdot i)$ [13]. The calculations of the filling factor were simplified neglecting the concentration of $\mathbf{B_1}$ by the high dielectric constant material like water. This is justified because the microwave magnetic field intensity is increased only by less than 5% in the presence of 0.4 mm thick layer of water positioned in the nodal plane as was calculated using the formulas developed by Hyde and Mett [13] or obtained from the high frequency structure simulator.

The results of calculations are plotted in Fig. 6. It follows from that plot that the optimum flat thickness for unsaturable aqueous samples is about 0.25 mm. It corresponds to the Q value drop to about 2/3 of the initial value in absence of water. This is in agreement with original conclusions of Wilmshurst [17] confirmed lately by Hyde and Mett [13].

In case of saturable samples the criteria for optimum flat cell thickness is different. Reduction of Q by the aqueous sample becomes a reduction of B_1. This allows an increase of incident power until the B_1 value reaches the same level. It can be easily shown

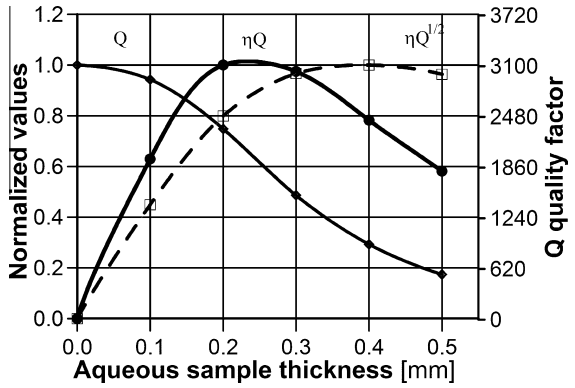

Fig. 6. Summary of calculations of the EPR signal amplitude as a function of aqueous sample thickness. A geometry of rectangular loop-gap resonator with a flat cell lying in the nodal plane was simulated. An optimum value of sample thickness for saturable samples appears at maximum of η and $\sqrt{Q}$ product (dashed line), whereas for non-saturable samples it is read from curve representing η and Q product (solid line). The dependence of quality factor Q on the sample thickness is also shown. All curves are normalized to the maximum value.

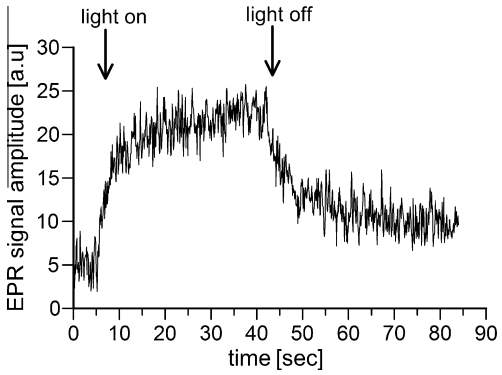

Fig. 7. The light-induced change of the EPR signal, measured in the time-sweep mode for the melanine placed within a modified RLGR. Sample exposition to the light is manifested as a instantaneous increase of the signal. When the light is switched off, the spin system relaxes to the previous state.

that in consequence the optimum flat cell thickness for saturable samples occurs at the maximum value of the product of η and $\sqrt{Q}$. It is seen from Fig. 6 that for the RLGR the maximum EPR signal for this kind of samples can be obtained when the flat cell thickness reaches about 0.4 mm. This corresponds to the drop in Q to 1/3 of its initial value similarly to TE_{102}, TM_{110} and TE_{U02} cavities [13].

Table 3 summarizes these considerations. The relative sensitivity for both saturable and non-saturable samples is explicitly calculated, thus performance of different resonators can be directly compared. Biophysical applications of EPR spectroscopy widely exploit saturable species (spin labels and other free radicals in aqueous solutions). In that case sensitivity of rectangular loop-gap resonator is not worse than conventional cavities, still preserving other benefits of loop-gap geometry.

7. The effect of illuminating the sample

Light can penetrate directly into the resonator due to holes created in the front side.

The sample is placed in a transparent flat cell, with dimensions matched to the inner space of the resonator. Geometrical calculations give an estimation of its exposed surface: it is about 50%. We chose synthetic dopa-melanin to observe the EPR signal induced by the light. This substance shows a broad absorbance over the UV and visible range, and gives a persistent EPR signal. After exposition to the visible light the recorded EPR spectrum is remarkably changed. First, the "dark" EPR signal has been recorded. Then the resonator loaded with the sample was exposed to visible light from a 250-W slide projector. The EPR spectrum of the illuminated sample was collected every 2 min. The remarkable increase of its amplitude can be observed immediately after the light is switch on. Results are presented in Fig. 7. The change of EPR signal amplitude measured in a "time-sweep" mode of the spectrometer is displayed.

Alternative solutions of the problem how to illuminate the sample within the EPR resonator were proposed as "miniature dielectric resonator" [18], or two-loop-one –gap structure with four holes [19]. Altough in the concept presented in [19] the light access inside the resonator also comes through the bored holes - the photoexcitable fraction of the sample volume is much lower compared to our structure.

8. Conclusions

The presented modification of the rectangular loop-gap resonator enables efficient illumination of the sample due to the extensive area of the light exposed surface and small thickness of the cell, still preserving a good EPR performance for aqueous solution. With that resonator the manageable volumes (10 times greater than for typical X-band 1 mm loop-gap) of the aqueous samples can be used. This is a substantial improvement for biophysical experiments. The modified resonator is characterized by good power conversion factor 2.5 $G/W^{1/2}$. The microwave magnetic field distribution in the nodal plane of the resonator is not disturbed by the presence of light access holes in the front side. Additionally, modifications introduced into the previous, basic structure of RLGR

Table 3
Relative sensitivity of EPR signal for aqueous samples in the flat cell with optimum thickness. There are compared: rectangular loop-gap resonator (RGLR), rectangular TE_{102} cavity and standard cylindrical TM_{110} cavity.

Type of resonator	$\left[G/\sqrt{W}\right]$	Sample width, w (mm)	Non-saturable samples		Saturable samples	
			Sample volume[a] ΔV (μL)	Relative signal from the whole sample[b] (%)	Sample volume[a] ΔV (μL)	Relative signal from the whole sample[c] (%)
RLGR	2.5[d]	4	12	95	19	38
TE102	0.99[e]	10	33	38	52	38
TM_{110}	1[f]	17	88	100	140	100

[a] ΔV = w.t. ΔL_{eff}, t is equal to 0.25 mm in case of non-saturable and 0.4 mm for saturable samples.
[b] Proportional to product of Λ^2, ΔV and δ and normalized with respect to TM_{110}.
[c] Proportional to product of Λ, ΔV and δ and normalized with respect to TM_{110}.
[d] Measured value for the empty resonator.
[e] Calculated value for the empty cavity with dimensions: 10 mm × 23 mm × 43.61 mm.
[f] Calculated value for the empty cavity. I.D. equals 38.49 mm and width – 18 mm.

[1] lead now to the slightly higher sensitivity as well as better thermal and mechanical stability. The wide application of this resonator is possible, e.g. biophysical experiments monitoring light-induced transient paramagnetic species or tracing light-induced conformational changes of spin-labeled biomolecules [20]. The high filling factor of the photoexcitable volume of the sample is achieved. Thus it can be the resonator of choice in biophysical experiments involving simultaneous illumination of the sample during its EPR signal recording.

Acknowledgments

This work was supported by the Grants: 3 P04A 043 23 from the State Committee for Scientific Research (Poland), and NIH 1-R03-EB007232-01A1. We thank dr Witold Korytowski for supplying us with the melanin samples.

References

[1] W. Piasecki, W. Froncisz, W.L. Hubbell, A rectangular loop-gap resonator for EPR studies of aqueous samples, J. Magn. Reson. 134 (1998) 36–43.
[2] J.S. Hyde, W. Froncisz, Loop-Gap Resonators, in: J. Hoff (Ed.), Advanced EPR in Biology and Biochemistry, Elsevier, Amsterdam, 1989.
[3] W.L. Hubbell, W. Froncisz, J.S. Hyde, Continuous and stopped-flow EPR spectrometer based on the loop-gap resonator, Rev. Sci. Instrum. 58 (1987) 1879–1886.
[4] L. Columbus, W. Hubbell, A new spin on protein dynamics, Trends Biochem. Sci. 27 (2002) 288–295.
[5] P.G. Fajer, Electron spin resonance spectroscopy labeling in peptide and protein analysis, in: R.A. Meyers (Ed.), Encyclopedia of Analytical Chemistry, John Wiley & Sons Ltd, Chichester, 2000, pp. 5725–5761.
[6] M. Sarewicz, S. Szytuła, M. Dutka, A. Osyczka, W. Froncisz, Estimation of binding parameters for the protein–protein interaction using a site-directed spin labeling and EPR spectroscopy, Eur. Biophys. J. 37 (2008) 483–493.
[7] J.S. Hyde, W. Froncisz, T. Oleś, Multipurpose loop-gap resonator, J. Magn. Reson. 82 (1989) 223–230.
[8] J. Ilnicki, J. Kozioł, T. Oleś, J. Kostrzewa, W. Galiński, R.J. Gurbiel, W. Froncisz, Saturation recovery EPR spectrometer, Mol. Phys. Rep. 5 (1994) 203–207.
[9] J.H. Freed, D.S. Leniart, J.S. Hyde, Theory of saturation and double resonance effects in ESR spectra. III. rf coherence and line shapes, J. Chem. Phys. 47 (1967) 2762–2773.
[10] W. Korytowski, B. Kalyanaraman, I.A. Menon, T. Sarna, R.C. Sealy, Reaction of superoxide anions with melanins: electron spin resonance and spin trapping studies, Biochim. Biophys. Acta Gen. Subj. 882 (1986) 145–153.
[11] W.S. Enochs, M.J. Nilges, H.M. Swartz, A standardized test for the identification and characterization of melanins using electron paramagnetic resonance (EPR) spectroscopy, Pigm. Cell Res. 6 (1993) 91–99.
[12] R.R. Mett, W. Froncisz, J.S. Hyde, Axially uniform resonant cavity modes for potential use in electron paramagnetic resonance spectroscopy, Rev. Sci. Instrum. 72 (2001) 4188–4200.
[13] J.S. Hyde, R.R. Mett, Aqueous sample considerations in uniform field resonators for electron paramagnetic resonance spectroscopy, Curr. Top. Biophys. 26 (2002) 7–14.
[14] J.S. Hyde, Signal amplitudes in electron paramagnetic resonance, varian associates technical information bulletin, Fall (1965) 10–13.
[15] EPR Resonator Characteristics, Bruker, 2003.
[16] G. Feher, Sensitivity considerations in microwave paramagnetic resonance absorbtion techniques, Bell Syst. Tech. J. 36 (1957) 449–484.
[17] T.H. Wilmshurst, Electron spin resonance spectrometers, Adam Hilger (Ed.), London, 1967.
[18] A. Blank, E. Stavitski, H. Levanon, F. Gubaydullin, Transparent miniature dielectric resonator for electron paramagnetic resonance experiments, Rev. Sci. Instrum. 74 (2003) 2853–2859.
[19] G. Elger, J.T. Törring, K. Möbius, Novel loop-gap probe head for time-resolved electron paramagnetic resonance at 9.5 GHz, Rev. Sci. Instrum. 69 (1998) 3637–3641.
[20] B. Knierim, K.P. Hofmann, O.P. Ernst, W.L. Hubbell, Sequence of late molecular events in the activation of rhodopsin, Proc. Natl. Acad. Sci. USA 104 (2007) 20290–20295.